Published in final edited form as:
Langmuir. 2010 November 16; 26(22): 17100–17110. doi:10.1021/la102642r.

Submicron Dropwise Condensation under Superheated and Rarefied Vapor Condition

Sushant Anand and **Sang Young Son***
Mechanical Engineering, School of Dynamic Systems, University of Cincinnati, Cincinnati, Ohio 45221

Abstract

Phase change accompanying conversion of a saturated or superheated vapor in presence of subcooled surfaces is one of the most common occurring phenomena in nature. The mode of phase change which follows such a transformation is dependent upon surface properties like as of contact angle and thermodynamic conditions of the system. In present studies, an experimental approach is used to study the physics behind droplet growth on a partially wetting surface. Superheated vapor at low pressures of 4–5 torr was condensed on subcooled silicon surface with static contact angle as of 60° in absence of non-condensable gases, and the condensation process monitored using Environmental Scanning Electron Microscope (ESEM) with submicroscopic spatial resolution. The condensation process was analyzed in the form of size growth of isolated droplets for before a coalescence event ended the regime of single droplet growth. Droplet growth obtained as a function of time reveals that the rate of growth decreases as the droplet increases in size. This behavior is indicative of an overall droplet growth law existing over larger time scales of which the current observations in their brief time intervals could be fitted in. A theoretical model based on kinetic theory further support the experimental observations indicating a mechanism where growth occurs by interfacial mass transport directly on condensing droplet surface. Evidence was also found which establishes the presence of submicroscopic droplets nucleating and growing in between microscopic droplets for partially wetting case.

INTRODUCTION

It is well known that many phenomena of common occurrence such as spreading of liquids, formation of droplets or thin films are governed by surface free energy interaction between the liquid and solid surface. Phase change processes involving liquid solid interaction such as condensation explicitly depend upon these surface energy interactions. Accurate calculation of surface energies is a tedious task involving computation of intermolecular interactions, so contact angle serves as a good indicator of defining the dynamics of a liquid-gas-solid system. Based on contact angle the liquid forms on a surface, condensation can be described as filmwise, dropwise or mixed condensation.1 For hydrophilic to super hydrophilic surfaces, a thin sheet of liquid film is formed upon condensation. This film offers an additional resistance for heat transfer between the solid surface and the gas and thereby limiting the amount of heat transfer that can take place across the wall. For hydrophobic surfaces there is instead a large bare surface in between condensing droplets which gives them a heat transfer coefficient which is 2–10 times more than filmwise

*Corresponding author: Phone: (513)556-5023, Fax number: (513) 556-3390, sangyoung.son@uc.edu.

SUPPORTING INFORMATION

The video recording of droplet growth on the bare Si surface at magnification of 250×, 500×, 6500× and 12000×. This material is available free of charge via the Internet at http://pubs.acs.org.

condensation.2 With a large nucleation site density (~ 10^8/cm^2 on smooth surfaces), it is possible to achieve high heat flux of 170–300 kW/m^2 in dropwise condensation mode.2,3

The extent of advantage that dropwise condensation has to offer makes it a more desirable mode of heat transfer as compared to filmwise condensation. However, dropwise condensation is notoriously tough to be maintained. Solutions to promote dropwise condensation primarily work on changing the surface energy of a solid surface by coating with chemicals such as dioctadecyl disulphide or oleic acid which give large contact angle (>120°).4–6 Ion implantation techniques have also been used to promote dropwise condensation mode.7, 8

In general, dropwise condensation depends upon several factors such as substrate orientation, thermal properties of substrate material, steam velocity, surface characteristics, wall subcooling and presence of non-condensable gases.9 These factors inherently affect several phenomenon associated with dropwise condensation such as droplet formation, size, nucleation density, drop size distribution and heat transfer coefficient. Understanding droplet formation and droplet growth kinetics is of utmost importance to develop a sound comprehension of vapor-liquid dynamics.

Based on previous experimental studies to observe the microscopic nature of droplet formation, two theories have been hypothesized to predict droplet formation. One hypothesis by Eucken treats dropwise condensation as a heterogeneous nucleation process with droplet embryos forming at nucleation sites while the intermediate area remains dry.10, 11 This theory postulates that all of the condensation takes place on the drops, while no more than monolayer exists in between the droplets. Experimental observations have established that dropwise condensation indeed begins as nucleation process.12, 13 The other hypothesis put forward by Jakob postulates that condensation begins in a filmwise manner initially covering the whole surface.14 This thin film ruptures after reaching a critical thickness (about 1 μm), where after droplets are formed. Meanwhile smaller droplets are drawn to adjacent droplets due to surface tension effect, while the droplets also grow simultaneously due to vapor-liquid transformation on them and coalescence. This model has also been supported by observations of others.15 Yongji, S., et al. also noted that a thin film of condensate exists in the area between the droplets, and while the droplets may depart this thin film remains.16

Although the pathways of droplet formation are still under debate, the theory of droplet condensation as a heterogeneous nucleation process has become widely accepted. Based on this hypothesis, several models have been proposed to describe the heat transfer for dropwise condensation. Theoretical models based on this model match to a great extent with the experimental observations. McCormick and Baer proposed a model in 1963 assuming vapor condensation to take place on submicroscopic areas.17 Gose. et al. proposed a model on which condensation occurs only on already formed droplets.18 Several other models were then introduced incorporating effects of coalescence, sweeping droplets, drop-size distributions etc.19 Griffith and Suk noted that surfaces having higher thermal conductivity have higher heat transfer rate for the same subcooling.20 They noted that the definition of heat transfer coefficient inherently makes dropwise condensation as a function of thermal conductivity of base material. Mikic however attributed this effect on non-uniform heat flux distribution around droplets and proposed “constriction resistance” as an important parameter affecting heat transfer.21 It was noted that dropwise condensation can be described if the drop-size distribution is known. Several attempts have been made in this regard.19, 22, 23 However the experimental limitations associated with using optical microscopes do not allow studying droplets smaller than 10 microns and as a result, the dropwise distributions are not available for the submicroscopic droplet regime. Obtaining

this information is critical as Graham and Griffith noted that at least 50% of heat transfer took place through drops which were less than 10 micron in diameter.24 Welch and Westwater further hypothesized that 97% of heat transfer was carried out by submicroscopic droplets or through bare area, while large droplets remained mostly absent in active heat transfer.15

Since dropwise condensation is a transient process where surface coverage of liquid on a substrate increases with time, studying droplet growth kinetics is vital to predict the associated transient nature of heat transfer. Different growth laws have been reported previously for describing growth of droplets with and without the coalescence. Initial condensation experiments on silanized surfaces with impinging water vapor showed the dependence as $R\alpha t^{1/4}$ for single droplet growth.25, 26 This was also supported by theoretical and numerical simulations which attributed this growth owing to diffusion of submicroscopic droplets under effect of concentration gradient.27 Later analysis showed that the dependence however to be $R\alpha t^{1/3}$ which was subsequently verified when the experiments were carried under gradual introduction of vapor.28–31 Experiments using non-polar liquid with very low contact angle have shown these drops growing to be linearly with time.32 It is clear that our understanding on mechanism and factors affecting droplet growth during condensation is not established fully.

The present work aims to show new evidence in regards to submicroscopic droplet formation and vapor to liquid transformation kinetics. Of special interest is studying the dynamics of vapor-liquid phase change under conditions of rarefied vapor environment. Lowering pressure increases the mean free path of the vapor molecules and hence the characteristic size of the minimum droplet size is increased. At 760 torr and 17 °C the mean free path (MFP) of water vapor is 0.11 μm, while at same temperature but at 4.2 torr MFP reaches 21.3 μm. Thus if there is an effect of mean free path on interfacial phase change kinetics, it is rendered visually noticeable in these conditions. Previous research for water vapor condensation suggests that at higher pressures drop conduction is the limiting resistance, while at the lower pressures interfacial heat transfer gains more importance.19, 33 A droplet growth model was presented by Umur based on kinetic theory wherein heat transfer through conduction was considered.11 Using the theory it was proved that interfacial heat transfer coefficient decreases by decreasing the operating pressure. Further the steam side heat transfer coefficient was found to decrease with decreasing pressure. This was supported by experimental observations.34, 35 However many aspects of vapor-liquid phase change remain unresolved owing to limitations of experimental setups such as spatial resolution, contamination issues, presence of non-condensable gases etc.

To overcome above mentioned limitations an Environmental Scanning Electron Microscope (ESEM) was used. Optical microscopes have limited spatial resolution which can be overcome using an electron microscope. ESEM is a relatively new development in the field of SEM operations. It combines the ability of Scanning Electron Microscope (SEM) to resolve objects at submicroscopic resolution with ability to perform dynamic experiments like condensation and evaporation by using water vapor as inside gas at lower pressures (2–20 Torr).

The construction details of an ESEM are widely available.36, 37 The availability of additional tools such as Peltier Cooler, Stress-Strain stage, micro injector and heater stage have extended the use of ESEM to more dynamical measurements. Although the physics behind the condensation-evaporation in ESEM has been investigated,38–40 application of ESEM towards studying fluid dynamics is a more recent phenomenon. Investigators have used ESEM to observe contact angles on fiber surfaces 41–43 for viewing aggregation and development of colloidal films.44, 45 Expressions have been developed to obtain contact

angles from the visual images obtained through ESEM wherever a droplet can be measured.46 More recently ESEM has been used towards studying fluid flows in carbon nanopipes.47–49 Only in recent times ESEM has been applied to study dynamical growth of droplets on different surfaces. Lauri et al.50 used ESEM to study droplet size growth on flat surfaces. Heterogeneous nucleation theory was used and the droplet size increment was measured and presented. Bhushan et al have used ESEM to observe transition effects of condensation and evaporation on patterned surfaces.51–53 ESEM images were analyzed and droplet size measurements obtained from the analysis to present size growth during condensation and droplet diameter decrease during evaporation.

While the lateral resolution to image samples is higher than normal optical microscopes, the imaging technique of ESEM gives a poor time resolution of order of seconds (1–10 sec). ESEM operation requires the chamber to be completely vented before introducing gas such as water vapor inside it. This effectively eliminates the probability of any non-condensable gas present in the chamber. This is of vital importance as experimental studies have shown that even small quantity of non-condensable gases results in significant deterioration in heat transfer performance by obstructing contact between vapor and the solid surface.54 The vapor inside the chamber is maintained at a particular pressure which is user controlled with help of computer. Further, the vapor inside carries negligible momentum and hence samples can be imaged without any surface shear effect due to vapor velocity. The rarefied environment inside the ESEM enhances the role of interfacial forces in vapor to liquid conversion.

By using this technique submicroscopic droplet formation and growth on a partially wetting Silicon surface was observed at much higher spatial resolution than reported elsewhere. Our primary aim is to study growth kinetics of a single droplet in a coalescence free regime, although we also present experimental results of droplet growth behavior in which coalescence and new intermittent droplet formation is also included. The experimental observations are supported by the droplet growth model of Umur and the implications of this are discussed in detail.

EXPERIMENTAL SETUP AND METHODOLOGY

The experimental setup used for the present studies is illustrated in Figure 1.

Bare Silicon wafer was used as condensation surface. A small piece (2 mm × 2 mm) of Silicon wafer was prepared and cleaned thoroughly using RCA cleaning process to remove any organic or inorganic contaminants present on the surface. Just before the experiment, the silicon wafer was dipped in Buffered Oxide Etched Solution for 30 seconds to remove any naturally formed SiO_2 layer on the wafer surface. Through this method contact angles of around 62 ± 2° were obtained for water on the silicon surface. A K-type thermocouple was planted on the Silicon surface using thermal epoxy to measure surface temperature. Due care was taken while application of the epoxy to the surface to prevent addition of large thermal mass while at same time maintaining proper contact between thermocouple tip and surface.

Experiments were carried inside Philips XL-30 Environmental Scanning Electron Microscope. It is equipped with vacuum pump and a vapor supply line which is linked with a glass bottle filled with DI water. At first, ESEM chamber is brought to a pressure approximately equal to 10^{-6} torr by the application of the vacuum pump. Then the vapor supply line is opened up. Because of the vacuum pressure inside the chamber and the supply line, the DI water in the glass bottle boils at room temperature and the vapor floods the ESEM chamber. The amount of vapor inside the chamber is computer controlled such that user designated pressure is maintained inside the chamber without significant fluctuations.

For surface cooling, a Peltier cooler stage was mounted inside the ESEM. Since the saturation vapor pressure is related to saturation temperature, a dynamical process such as water condensation can be studied in ESEM by using the Peltier cooler in conjunction with controlling the pressure and consequently the Relative Humidity (RH) in the ESEM chamber. When RH>100%, condensation can be observed immediately. Thermodynamically, the saturation vapor pressure and temperature dependence for ESEM is shown in Figure 2. The saturation vapor pressure-temperature curve of ESEM differs from the standard curve because the temperature of the vapor T_V above the sample is different from the sample temperature T_S. The thermodynamic relation between the saturation vapor pressure and temperature for condensation to take place can be expressed by the Eqn (1) as given by Cameron and Donald55

$$P_w = \left(\frac{T_s}{T_v}\right)^{0.5} P_{sat}(T_s) \tag{1}$$

Where, $P_{sat}(T_S)$ is saturation vapor pressure at temperature T_S.

Since the vapor inside the ESEM chamber had originated from the boiling of water under low pressure, and the water temperature was maintained at ambient, the vapor temperature is same as water temperature in the glass bottle (around 17 °C). Thus with respect to the pressure inside the chamber (around 4.2 torr), the vapor is in superheated condition.

The Philips XL30 ESEM has a K-Type thermocouple connector available which was used in our studies. It was connected with the K-type thermocouple attached on Si surface and externally connected to a Data Acquisition Device (Agilent 34970A). A LabView™ program was used to monitor the thermocouple temperature and save the data on computer. Initially to test the peltier readout, it was attached with the peltier surface. Substantial temperature difference between the thermocouple and temperature shown by the peltier cooler was observed. As a result it was decided to use K-type thermocouple as the basis for calculating the saturation vapor pressure-temperature curve. According to the theoretical predictions, the saturation temperature at 4.2 torr is −0.675 °C. However, using the K-type thermocouple, the temperature at which condensation at 4.2 torr of vapor pressure was found to be −0.5 °C. In absence of proper calibration of the thermocouple and the inherent uncertainty in K-type thermocouple (+/− 0.5 °C), this degree of temperature difference can be anticipated in the measurements.

Droplet growth was visualized in two ways with respect to substrate plane – from the top and from an almost vertical stance. For observing the substrate on the top, it was attached to the peltier surface using thermally conductive carbon tape. A special copper stage was prepared to rest on the peltier cooler to observe growth of droplets from side view to observe contact angle changes. The copper stage had an inclined surface of 80° as shown in Figure 3. The bare silicon wafer was placed on the inclined surface using thermally conductive carbon tape. In this arrangement, the thermocouple was attached with copper stage instead of Silicon surface to allow proper viewing.

The imaging of specimen inside the chamber was done using Gaseous Secondary Electron Detector (GSED). The ESEM imaging involves an electron beam scanning across a given area. Electron beam parameters like dwell time and scan rate decide the amount of time taken to scan a given area visible on screen. These parameters were adjusted and a small area was selected to give a scan time of 2–10 seconds with adequate clarity. The imaging detector feeds live images to the computer. A BNC video output was used to divert the

image signals to a Sony DVCAM, and live video recording was done. The timing of the DVCAM was manually synchronized with computer to match temperature conditions with associated imaging signal.

Once the system was setup, the first step involved venting the chamber and filling it with pure water vapor. An eight cycle pumpdown sequence between 0.5 torr to 9 torr was performed to make sure air is properly vented out and chamber is filled with saturated vapor pressure in the end.55 The presence of a foreign surface in vicinity of metastable vapor lowers the energy barrier required to cause nucleation as compared to homogeneous nucleation.31 Characteristics such as contact angle, defects, and scratches influence the nucleation capability on a surface. Thus, at the same pressure, dropwise condensation can occur at slightly higher temperature than predicted by the theoretical modified equation. It was noted that in rough regions along the edges of the substrate, condensation began at a still higher temperature than shown in Figure 2. Clearly, the micro-cavities or edges were sites of much lowered surface energy barrier which resulted in this phenomenon.

Once the pumpdown was performed, condensation can be initiated by manipulating chamber pressure and peltier temperature which were also the controlling parameters. This condensation process was recorded at different magnifications (250×, 500×, 1500×, 3500× and 6500×) and for accelerating voltage of 15 keV. The observation of submicroscopic droplets requires higher beam voltage for sharper contrast, thus the beam voltage was increased to 25 keV for better visualization. Since the removal of condensing droplets cannot be imposed inside the experimental setup, so condensation once triggered eventually leads to complete surface coverage of the substrate. An area was selected randomly to observe a droplet growth. After the droplet merged with another droplet, the focus of electron gun was moved to another area to observe another droplet which had a higher probability of growing without merger because of lesser population density of droplets around it. With this method, droplet growth histories were recorded for different droplets at different stages of their growth. The choice of electron beam voltage was based on determination of best contrast for visualization, while also minimizing any effect of beam heating. Hence these experiments were carried at 15 keV.

Post processing results involved image analysis to determine droplet growth rate which was done using ImageJ software.56 The controlling parameters for the study were chamber pressure and the peltier cooler temperature.

RESULTS AND DISCUSSION

a) Method of condensation

As mentioned above, the condensation process can be triggered by controlling the pressure and temperature. In particular, there are two methods to achieve condensation:

Mode 1- Constant vapor pressure, varying substrate temperature. The pressure is fixed and the temperature is slowly decreased to initiate dropwise condensation

Mode 2- Constant substrate temperature, varying vapor pressure. The temperature of the peltier cooler is fixed and the pressure is slowly increased until condensation process starts.

We found that the droplet growth and coalescence results were affected to some extent by the method to achieve condensation. This happened because of its influence on the time required to achieve a steady state.

It was observed that temperature control was much more difficult in the first mode. This resulted in non-uniform droplet growth. On the other hand, the second mode gave a more

uniform temperature profile and the time required to reach steady state was drastically reduced. In this mode, a more uniform model of coalescence and droplet growth was achieved which is discussed in the following sections.

b) Effect of Beam Heating

Since the mechanism of imaging in ESEM involves line scan of an electron beam over the surface, the impinging electrons can cause instantaneous heating of the spot at which impingement is occurring. Although the beam current may be less and the electron beam diameter is of order of nanometers, this can result in a very high dosage of electrons concentrated over a very small area and hence high heat flux may ensue. If the beam heating is significant, it can affect the condensation process. To ascertain the effect of beam heating, a 100 μm junction diameter thermocouple wire (Figure 4) was inserted in the ESEM chamber and was exposed to electron beam under vacuum conditions (pressure ~10^{-6} torr).

Two modes are possible – spot mode and line scan mode and both of these modes were chosen to evaluate the effect of heating. It was found that beam heating was dependent upon several factors such as line time, beam voltage, mode type and spot size. Figure 5 shows the effect of beam heating with line scan mode and spot mode (for spot size 3) on thermocouple tip.

In general it was found that spot mode produced higher amount of heating and a larger spot size produced larger amount of heating. A maximum of 0.5 K of heating was observed under the spot mode for the current operating conditions. Increasing the spot size in general led to increase in temperature.

For imaging purposes, the map scan mode was used during the experiment which involved electron beam rastered across an entire chosen area. For current chosen conditions of 15 keV beam voltage and line time of 16.7 ms, it can be observed that beam heating is of order of 0.1 K. Increasing the beam voltage to 25 keV resulted in beam heating to the order of 0.3 K. It should be noted that current beam heating experiment was performed on a thermocouple tip which is of thermally and electrically conducting in nature.

On insulating materials, the effect of concentrated beam of electrons may be different from present observations. Under ESEM conditions the electron beam width is enhanced to the order of μm because of collision events of electrons with vapor molecules inside.[57, 58] Thus the dosage of electrons reaching a spot is greatly reduced and it can be expected that beam impingement would have negligible heating effect.

c) Dropwise Growth for single droplets –experimental results

As mentioned previously, understanding evolution of a single droplet can provide us with understanding of heat transfer through the droplet which can then be used to evaluate over all heat transfer. The droplet growth may occur by different mechanisms depending upon physical and thermodynamic conditions such as.[31]

- **i.** Direct phase change of vapor to liquid at the drop surface.
- **ii.** Thermal release of interphase mass conversion can lead to Marangoni forces which trigger temperature gradients inside the droplet. This can induce local subcooling at droplet periphery so probability of vapor condensation increases along the periphery.
- **iii.** Nucleation and growth of the droplets by means of surface diffusion. This has widely been observed for water on several substrates. Experimental observations by others have led to a generalized droplet growth model of $D = kt^n$ where D is the

droplet diameter growing over a period of time t and n and k are empirical constants. The value of n has been reported as 1/3 or 1/4 in cases where surface diffusion is a prominent mechanism.[28–31]

Irrespective of the mechanism involving how a droplet evolves, the condensational growth of droplet formation is a multi-stage process.[29] The first stage involves droplet growth of single and individual droplets wherein a number of nucleation sites may become active. This stage is marked by low surface coverage. As droplets grow in size, the inter-droplet distance decreases until the droplets meet together, where after the combined effect of surface tension and growth leads to coalescence of these droplets. This is referred to as second stage in the growth. Beyond this, in third stage more coalescence may occur and new droplets may be nucleated in the bare area between the droplets.

The essential aim of this study was to understand the first stage involving how an individual droplet evolves over time. However measuring droplet growth for single droplets over an extensive period of time is significantly difficult because the time for droplet interaction leading to coalescence is very short – lasting only to few number of frames. Droplet interaction depends upon the degree of subcooling with larger subcooling initiating an increased number of nucleation sites and hence increasing the population density of droplets on the surface. This then results in significant coalescence events and a much shorter time period where a single droplet can evolve without interaction from neighboring droplets. Thus to record substantial period of growth devoid of the coalescence behavior is a challenge. Using a very low degree of subcooling the number of population sites can be controlled. Further, lower degree of subcooling also decreases the droplet growth which can further help in observation of droplet evolution over a larger period of time.

The temperature of the vapor inside the ESEM chamber is 17 °C, while the temperature at which condensation occurs is −0.675 °C. From this information and by usual convention, it can be affirmed that the degree of subcooling is 17.675 °C. However, it should be noted that the presence of peltier cooler establishes a temperature gradient around the substrate. Around the substrate ~O(μm), the temperature of the vapor molecules is much closer to the actual peltier cooler. Thus the effective degree of subcooling is much lower when the peltier cooler is active. Accurate prediction of the degree of subcooling can be made by measuring temperature of vapor just above the peltier cooler surface. Since an additional thermocouple measurement cannot be incorporated in the experimental setup, prediction of effective degree of subcooling was not achievable. By controlling the peltier cooler temperature, we were able to locate and measure droplets growing on their own without merger for time periods in the range of 40–180 seconds.

Figure 6, shows a series of frame containing condensed droplets at 500× magnification on Silicon surface.

Each droplet was identified with the initial peripheral diameter measured as the diameter of the droplet in the first frame of a series of frames where the droplet was observed to grow over a period of time. As mentioned previously, the time between successive growths is dependent upon the area and the scan rate of the electron beam. Thus growth record of each droplet was obtained using this technique. Figure 7 is an indicative plot of droplet growth as a function of time for the three different droplets showed in Figure 6. The different droplets are identified based on the initial diameter.

The growth curve as shown in Figure 7 was found to be characteristic of droplets evolving under conditions under study. After careful analysis, many characteristics were revealed on the nature of droplets. As can be seen from Figure 7, the droplet diameter appears to grow linearly with time. A similar linear pattern was also observed when the data was plotted in

terms of droplet area (D^2) with time, thereby giving an impression that $D^2 = kt$. After careful consideration the perplexing nature of the observed drop diameter growth pattern was resolved, when it was noted that the rate of diameter growth was different for different droplets. As can be seen the rate of growth (dD/dt) was noted to decrease as the diameter of the droplet increase.

The linear nature of diametrical growth for all the droplets gives a certain ambiguity to this observation. The situation becomes clearer when the diameter was observed on a logarithmic scale as shown in Figure 8. From Figure 8, it becomes unambiguously clear that the rate of diametrical growth for smaller droplets is much higher than the rate at which larger droplets appear to grow. Moreover, the droplet diametrical growth rate appears to change as the droplet size reaches near the size of mean free path of vapor molecules in the chamber.

However to understand the mechanism behind this behavior it is essential to identify an overall growth pattern where each of the droplet growth patterns can be fitted in. It is clear that droplet evolution observed for a period of 40 – 100 seconds was not enough to predict the mechanism by observing how one of the many single droplets was growing.

For this purpose, a scheme was employed to visualize droplets observed at different times and different stages of growth as a single droplet growth curve. From the records of droplet growth, the droplet with smallest initial diameter (D_{01}) analyzed was identified. Using polynomial fitting, a fourth order equation was fitted into this curve to obtain a relation between diameter and time. Then the droplet with next smallest initial diameter (D_{02}) was chosen to fit into the polynomial curve of the earlier droplet for identifying the time t_{02} at which D_{02} would coincide. After identifying t_{02} the entire series of D_{02} was incremented in time by t_{02} to obtain the next curve. This process was repeated to interpolatively fit each individual droplet into the previous curve. For much larger droplets, where a pre-existing curve was not found to fit their diameters, an extrapolative scheme was used to identify the time increment with an understanding that this extrapolation scheme may not as accurate as the interpolative scheme. Using this scheme an overall droplet growth pattern could be observed as shown in Figure 9.

From Figure 9, it can be seen that the interpolative scheme provides a good fit to an overall trend, while for larger diameters; the time increment provided by the extrapolation method may not be as accurate. These results can be improved by obtaining droplets growing in the intermittent size range, however even in our record of over 100 single droplets with substantial growth, the droplets in between these size ranges were missing. The larger the droplet grows the probability of coalescence increases and when coalescence happens, there is a sudden jump in droplet growth due to which intermediate droplets could not be isolated. From Figure 8 and Figure 9, it can be seen that under the experimental conditions, a droplet took a prolonged time (~90 seconds) to grow from 1 μm to 25 μm.

The behavior of droplet diameter growth provides an insight into the vapor-phase transformation which can be understood by application of principles of kinetic theory of gases.

d) Dropwise Growth for single droplets – Theory

The key to understand behavior of the observed droplet diameter growth is identifying the mechanics of vapor-liquid transformation. For steam-water transformation the most common occurring mechanism of this transformation involves diffusional growth. This conjecture is supported by high magnification images (such as shown in Figure 14) which show presence of nano sized droplets along the periphery of the growing micro-sized

droplets. These were observed to merge into the larger droplet. Thus diffusion of nano-droplets due to capillary imbibition is clearly active during the process of dropwise growth. The rate of growth if this mode alone is active is given by $D=kt^{0.33}$.28–31 However a large discrepancy was found when the recorded data from present studies was tried to fit with this growth law. It became clear that diffusional growth cannot solely account for the droplet growth pattern observed in present case.

The kinetics of vapor-liquid phase change behavior observed under present experimental studies can be explained by application of principles of kinetic theory of gases. The following analysis is based on dropwise condensation theory developed by Umur.12 In the following analysis, the effects of disjoining pressure and extended meniscus around the droplet are neglected. Also in the accompanying theory, the nucleation characteristics of the surface are not discussed and it is assumed that the droplet has already nucleated.

A single droplet sitting on a surface at temperature T_l is considered and surrounded by vapor at temperature T_v and pressure at P_v (Figure 10). The vapor-liquid interface temperature is assumed to be T_i.

The volume and the exposed surface area of the droplet sitting on the surface with contact angle θ is given by

$$V=\frac{\pi R^3(2+\cos\theta)(1-\cos\theta)^2}{3} \tag{2}$$

$$A=2\pi R^2(1-\cos\theta) \tag{3}$$

While the area of the droplet base is given by

$$B=\pi R^2\sin^2\theta \tag{4}$$

At the droplet interface, impinging vapor molecules escape into the vapor region. The imbalance between influx and out flux of water molecules gives the net rate of droplet growth or dissipation. In particular, the net mass flux rate at a surface is given by

$$\dot{m}''=\dot{m}_v''-\dot{m}_l'' \tag{5}$$

The condensation term can be given by

$$\dot{m}_v''=\frac{\alpha_c p_v}{\sqrt{2\pi T_v \overline{R}/M}} \tag{6}$$

The most significant aspect of the above equation is the condensation accommodation coefficient. Condensation coefficient (α_c) defines the probability of a water molecule to stick to the condensing surface or in other words become a part of the condensate. Thus ($1-\alpha_c$) signifies the molecules which are reflected back to the vapor state. Substantially lower

values of condensation coefficient signify much larger interfacial resistance and a larger temperature jump.59

Because it is assumed that the vapor-liquid interface is at a temperature T_i, it implies inclusion of a temperature jump condition at the interface. To analyze this problem, the evaporative component can be given by Boltzmann law.60

$$\dot{m}_l'' = \dot{m}_0'' f_s Exp\left(-\frac{\lambda_s}{\bar{R}T_v}\right) \tag{7}$$

The above two equations can be solved in conjunction with heat transfer accompanying the phase change. If heat transfer is considered between vapor, condensing liquid and the substrate, then

$$q_d = h_e A(T_v - T_i) = h_d B(T_i - T_l) \tag{8}$$

The interfacial heat transfer coefficient is related to the mass transfer occurring at the liquid-vapor interface and is given by

$$h_e = \frac{\dot{m}'' \lambda_s}{T_v - T_i} \tag{9}$$

The drop side coefficient h_d can further be calculated using the drop distribution function by Mccormick and Baer.17

$$\frac{D_{Base} h_d}{k_l} = \frac{8}{\theta}\int_0^{D/2} \frac{x dx}{(D/2)^2 - x^2} \approx \frac{9.2}{\theta} = f(\theta) \tag{10}$$

The above equations can be combined to eventually lead to

$$R^2 - R_0^2 + f_2(\theta) f(s)\left\{R - R_0 + R^* \ln\left(\frac{R - R^*}{R_0 - R^*}\right)\right\} = \eta_1 t$$

where

$$\begin{aligned} \eta_1 &= \frac{k_l(T_v - T_l)}{f_1(\theta)\rho_l \lambda_s} \\ f_1(\theta) &= \frac{(2+\cos\theta)(1-\cos\theta)^2}{\sin\theta f(\theta)} \\ f_2(\theta) &= \frac{(1+\cos\theta) f(\theta)}{2\sin\theta} \\ f(s) &= \frac{2-\alpha_c}{2\alpha_c} \frac{\sqrt{2\pi} k_l (\bar{R}/M)^{1.5} T_v^{2.5}}{p_v \lambda_s^2} \\ f(\theta) &= \frac{9.2}{\theta} \end{aligned} \tag{11}$$

The above solution is a mixed solution of linear and exponential terms. As mentioned previously, a very critical parameter in determining the solution for the above equation is the condensation accommodation coefficient α_c. Various methods employed in literature give a wide range of suitable values of α_c.61 Typically it is expected that in pure vapor conditions, α_c is closer to 1, while at lower pressures its value is expected to be lesser than 1.

Evaluating condensation coefficient during condensation experiments is a challenge owing to presence of non-condensable gases and contaminations. However as explained previously, the rarefied environmental conditions inside ESEM are conducive for such measurements. The experimental technique along with the presented theory can be used to evaluate condensation coefficient. Although the current setup and the method can be used to determine condensation accommodation coefficient, there remains ambiguity regarding the true value on account of uncertainty in temperature measurement.

By adjusting α_c and degree of subcooling ($T_v - T_l$), a fit was obtained to match the theoretical results with the experimental values (Figure 11).

The fit was obtained for an accommodation coefficient of 0.8 and a degree of subcooling of 0.006 °C. As has been stated before, the effective degree of subcooling for the present setup cannot be measured experimentally. Eqn. 10 illustrates the growth rate does not have a direct dependence upon the temperature of the substrate. Instead the growth rate is affected by the degree of subcooling given by temperature difference of the vapor and the substrate. Thus, the diametrical growth rate is not sensitive to the experimental temperature uncertainties of the substrate temperature. The much lower value of the effective degree of subcooling for the theoretical fit reflects the conjecture that only the molecules near the substrate contribute in phase change process. The molecules far away from the peltier cooler are much more energetic than the molecules near the substrate surface and hence do not play active role in condensation process. This further indicates that the degree of temperature jump near the liquid-vapor interface is negligible and thus the interfacial resistance is very small. Moreover, the temperature conditions inside the droplet are nearly isothermal with negligible temperature difference between the substrate surface (T_s) and the interfacial temperature (T_i) at the droplet perimeter.

From the theoretical principles leading to conformity with experimental observations, it becomes clear that under the conditions of ESEM, the droplet growth occurs directly by mechanism of conversion of vapor to the liquid medium. From Figure 11, it can be seen that droplet diameter growth rate observed during the experiment evidently changes as the droplet diameter approaches the mean free path of vapor molecules. However, this observed relevance of mean free path of vapor molecules on droplet growth is not captured in the dropwise condensation theory by Umur and requires further investigation.

e) Dropwise Growth for coalescing droplets

The specially built copper stage was used to observe coalescence behavior and observe change in contact angle. Figure 12 shows an example of the droplet growth captured on the Silicon surface attached to the copper stage.

Figure 13 shows the results of droplet diameter growth rate at 4.2 torr wherein substrate temperature was held steady and vapor pressure was increased to initiate condensation. An average diameter was computed based on visible droplets in a given frame as per equation given below

$$(D_{avg})_{frame} = \sum_{1}^{n} D_i / n \tag{12}$$

The diameter and contact angle of each droplet was calculated using LBADSA plugin in ImageJ.62

As seen, there was a sudden jump in droplet diameter when coalescence took place. Depending upon the number of coalescing events, the jump could be much higher. It was noticeable that after coalescence, the droplets continued to grow at same diametrical rate law as of a single droplet growth until the next coalescence took place. Another distinct pattern observable under present experimental situation was the birth of a new generation of droplets in between coalescence times. Even when the drops had been nucleated and were growing, new droplets nucleated at different period of times. A substantial decrease in the average diameter $(D_{avg})_{frame}$ is indicative of large number of new droplets which nucleate in a given frame. This is clear from Figure 13, where new droplet formation shows a decrease in average diameter, and a coalescence event led to increase in average diameter in an image frame.

By observing the condensation process on the specially built copper stage, it was observed that coalescence and the droplet growth were accompanied by a change in dynamic contact angle. Particularly during the coalescence, the contact angle change depends upon the volume of merging droplets and degree of their separation. Surface forces acting on the droplet are active during all the time, and as such when droplets merge there exists a brief period during which the combined droplet tries to adjust its center of mass to satisfy those forces by overcoming frictional forces. As noted, the droplet edges are pinned down due to frictional forces due to which the combined droplet requires some time to return to its normal state.63

f) Submicroscopic droplet visualization

Droplets were found to nucleate at the same spot which reinforces the idea that condensation is a heterogeneous nucleation phenomenon. As can be seen from Figure 14, submicroscopic droplets were found to be nucleating and growing in between larger droplets for our case.

As mentioned previously, most of present models on dropwise condensation are based on premise that condensation occurs primarily on the droplets with little or no condensation on portions of the surface between droplets. However it is clear from Figure 14, that this assumption needs a revisit. Whether the formation of submicroscopic droplets occurs everywhere at the very beginning of first wave of droplet formation cannot be postulated yet. However it can be seen that the ‘bare area’ is populated entirely by submicroscopic droplets of different sizes.

Even further, from Figure 14, presence of sub-microscopic droplets appearing, growing and then coalescing with the larger droplet can be observed. Some of the nanodroplets can be seen sitting ~ 100 nm from the larger droplet. The role of surface tension appears certainly an important one to cause diffusion/migration of micro/nano droplets into the bigger droplet.

CONCLUSION

Dropwise condensation was studied in a superheated environment and rarefied vapor condition at as low as of 4 torr using an Environmental Scanning Electron Microscope. Droplet growth of single droplets was studied along with their coalescence behavior with

other droplets. The analysis of experimental observation reveals a mechanism where growth of droplets occurs directly by means of vapor to liquid conversion on the droplet itself. Numerical simulations on droplet growth using a theoretical model based on kinetic theory of gases provide a deeper understanding of interfacial mass transport under the experimental conditions. In particular the diameter of the droplet growth was found to decrease as the droplet diameter increases. Evidence was also found which establishes presence of submicroscopic droplets nucleating and growing in between microscopic droplets for partially wetting case.

Supplementary Material

Refer to Web version on PubMed Central for supplementary material.

Acknowledgments

The study presented was supported by Grant Number U01ES016123 from the National Institute of Health (NIH). The content is solely the responsibility of the authors and does not necessarily represent the official views of the National Institute of Environmental Health Sciences or the National Institutes of Health (NIH). We thank Dr Doug Kohls and Mr. Ratandeep Singh Kukreja of the Advanced Materials Characterization Center (AMCC) at University of Cincinnati for their invaluable help in ESEM measurements.

References

1. Ma X, Rose JW, Xu D, Lin J, Wang B. Advances in dropwise condensation heat transfer: Chinese research. Chemical Engineering Journal. 2000; 78(2–3):87–93.
2. Bejan, A.; Kraus, AD. Heat transfer handbook. Wiley-Interscience; 2003.
3. Cengel, YA. Heat transfer: a practical approach. McGraw-Hill Companies; 2003.
4. Rose JW. Condensation heat transfer. Warme- und Stoffubertragung Zeitschrift. 1999; 35(6):479–485.
5. Vemuri S, Kim KJ. An experimental and theoretical study on the concept of dropwise condensation. International Journal of Heat and Mass Transfer. 2006; 49(3–4):649–657.
6. Holden KM, Wanniarachchi AS, Marto PJ, Boone DH, Rose JW. The use of organic coatings to promote dropwise condensation of steam. Journal of heat transfer. 1987; 109(3):768–774.
7. Zhao, Q.; Burnside, BM. Heat Recovery Systems & CHP. September. 1994 Dropwise condensation of steam on ion implanted condenser surfaces.
8. Bani Kananeh A, Rausch MH, Fröba AP, Leipertz A. Experimental study of dropwise condensation on plasma-ion implanted stainless steel tubes. International Journal of Heat and Mass Transfer. 2006; 49(25–26):5018–5026.
9. Abdelmessih AH, Neumann AW, Yang SW. The effect of surface characteristics on dropwise condensation. Letters in Heat and Mass Transfer. 1975; 2(4):285–291.
10. Eucken A. Energie-und Stoffaustausch an Grenzflächen. Naturwissenschaften. 1937; 25(14):209–218.
11. Carey, VP. Liquid-vapor phase-change phenomena. 2. Taylor & Francis; 2006.
12. Umur, A.; Griffith, P. Mechanism of dropwise condensation. Massachusetts Institute of Technology, Dept. of Mechanical Engineering; 1963.
13. McCormick JL, Westwater JW. Nucleation sites for dropwise condensation. Chemical Engineering Science. 1965; 20(12):1021–1036.
14. Jakob, M. Heat transfer in evaporation and condensation. University of Illinois; 1937.
15. Welch JF, Westwater JW. Microscopic study of dropwise condensation. International Developments in Heat Transfer. 1961; 2:302–309.
16. Yongji S, Dunqi X, Jifang L, Siexong T. A study on the mechanism of dropwise condensation. International Journal of Heat and Mass Transfer. 1991; 34(11):2827–2831.
17. McCormick JL, Baer E. On the mechanism of heat transfer in dropwise condensation. Journal of Colloid Science. 1963; 18(3):208–216.

18. Gose EE, Mucciardi AN, Baer E. Model for dropwise condensation on randomly distributed sites. International Journal of Heat and Mass Transfer. 1967; 10(1):15–22.
19. Rose JW. On the mechanism of dropwise condensation. International Journal of Heat and Mass Transfer. 1967; 10(6)
20. Griffith P, Man Suk L. The effect of surface thermal properties and finish on dropwise condensation. International Journal of Heat and Mass Transfer. 1967; 10(5):697–707.
21. Mikic BB. On mechanism of dropwise condensation. International Journal of Heat and Mass Transfer. 1969; 12(10):1311–1323.
22. Le Fevre, EJ.; Rose, JW. A theory of heat transfer by dropwise condensation. Proceedings of the Third International Heat Transfer Conference; 1966; 1966. p. 362-375.
23. Abu-Orabi M. Modeling of heat transfer in dropwise condensation. International Journal of Heat and Mass Transfer. 1998; 41(1):81–87.
24. Graham C, Griffith P. Drop size distributions and heat transfer in dropwise condensation. International Journal of Heat and Mass Transfer. 1973; 16(2):337–346.
25. Beysens D, Knobler CM. Growth of Breath Figures. Physical Review Letters. 1986; 57(12):1433–1436. [PubMed: 10033448]
26. Fritter D, Knobler CM, Beysens DA. Experiments and simulation of the growth of droplets on a surface (breath figures). Physical Review A. 1991; 43(6):2858–2869. [PubMed: 9905351]
27. Rogers TM, Elder KR, Desai RC. Droplet growth and coarsening during heterogeneous vapor condensation. Physical Review A. 1988; 38(10):5303–5309. [PubMed: 9900252]
28. Briscoe BJ, Galvin KP. An experimental study of the growth of breath figures. Colloids and Surfaces. 1991; 56(C):263–278.
29. Beysens D. The formation of dew. Atmospheric Research. 1995; 39(1–3):215–237.
30. Zhao H, Beysens D. From Droplet Growth to Film Growth on a Heterogeneous Surface: Condensation Associated with a Wettability Gradient. Langmuir. 1995; 11(2):627–634.
31. Beysens D. Dew nucleation and growth. Comptes Rendus Physique. 2006; 7(9–10):1082–1100.
32. Gokhale SJ, Plawsky JL, Wayner PC Jr. Experimental investigation of contact angle, curvature, and contact line motion in dropwise condensation and evaporation. Journal of Colloid and Interface Science. 2003; 259(2):354–366. [PubMed: 16256516]
33. Hiroaki T, Takaharu T. A microscopic study of dropwise condensation. International Journal of Heat and Mass Transfer. 1984; 27(3):327–335.
34. Tanner DW, Pope D, Potter CJ, West D. Heat transfer in dropwise condensation at low steam pressures in the absence and presence of non-condensable gas. International Journal of Heat and Mass Transfer. 1968; 11(2)
35. Shigeo H, Hiroaki T. Dropwise condensation of steam at low pressures. International Journal of Heat and Mass Transfer. 1987; 30(3):497–507.
36. Danilatos GD. Introduction to the ESEM instrument. Microscopy research and technique. 1993:25.
37. Danilatos GD. Mechanisms of detection and imaging in the ESEM. Journal of microscopy(Print). 1990; 160:9–19.
38. Cameron RE, Donald AM. Minimizing sample evaporation in the environmental scanning electron microscope. Journal of Microscopy. 1994; 173:227–237.
39. Meredith P, Donald AM. Study of ‘wet’ polymer latex systems in environmental scanning electron microscopy: Some imaging considerations. Journal of Microscopy. 1996; 181(1):23–35.
40. Thiel BL, Donald AM. The study of water in heterogeneous media using environmental scanning electron microscopy. Journal of Molecular Liquids. 1999; 80(2–3):207–230.
41. Wei Q, Mather RR, Fotheringham AF, Yang RD. Observation of wetting behavior of polypropylene microfibers by environmental scanning electron microscope. Journal of Aerosol Science. 2002; 33(11):1589–1593.
42. Wei QF, Mather RR, Fotheringham AF, Yang RD. ESEM study of wetting of untreated and plasma treated polypropylene fibers. Journal of Industrial Textiles. 2002; 32(1):59–66.
43. Wei Q, Liu Y, Wang X, Huang F. Dynamic studies of polypropylene nonwovens in environmental scanning electron microscope. Polymer Testing. 2007; 26(1):2–8.

44. Donald AM, He C, Royall CP, Sferrazza M, Stelmashenko NA, Thiel BL. Applications of environmental scanning electron microscopy to colloidal aggregation and film formation. Colloids and Surfaces A: Physicochemical and Engineering Aspects. 2000; 174(1–2):37–53.
45. Donald AM. The use of environmental scanning electron microscopy for imaging wet and insulating materials. Nature Materials. 2003; 2(8):511–516.
46. Brugnara M, Della Volpe C, Siboni S, Zeni D. Contact angle analysis on polymethylmethacrylate and commercial wax by using an environmental scanning electron microscope. Scanning. 2006; 28(5):267–273. [PubMed: 17063765]
47. Pía Rossi M, Ye H, Gogotsi Y, Babu S, Ndungu P, Bradley JC. Environmental scanning electron microscopy study of water in carbon nanopipes. Nano Letters. 2004; 4(5):989–993.
48. Rossi MP, Gogotsi Y. In situ ESEM study of liquid transport through carbon nanopipes. Microscopy and Microanalysis. 2004; 10(SUPPL. 2):1054–1055.
49. Yarin AL, Yazicioglu AG, Megaridis CM, Rossi MP, Gogotsi Y. Theoretical and experimental investigation of aqueous liquids contained in carbon nanotubes. Journal of Applied Physics. 2005; 97:124309.
50. Lauri A, Riipinen I, Ketoja JA, Vehkamäki H, Kulmala M. Theoretical and experimental study on phase transitions and mass fluxes of supersaturated water vapor onto different insoluble flat surfaces. Langmuir. 2006; 22(24):10061–10065. [PubMed: 17107000]
51. Bhushan B, Jung YC. Wetting adhesion and friction of superhydrophobic and hydrophilic leaves and fabricated micro/nanopatterned surfaces. Journal of Physics Condensed Matter. 2008; 20(22)
52. Jung YC, Bhushan B. Wetting behaviour during evaporation and condensation of water microdroplets on superhydrophobic patterned surfaces. Journal of Microscopy. 2008; 229(1):127–140. [PubMed: 18173651]
53. Zheng Y, Han D, Zhai J, Jiang L. In situ investigation on dynamic suspending of microdroplet on lotus leaf and gradient of wettable micro- and nanostructure from water condensation. Applied Physics Letters. 2008; 92(8)
54. Le Fevre EJ, Rose JW. An experimental study of heat transfer by dropwise condensation. International Journal of Heat and Mass Transfer. 1965; 8(8):1117–1133.
55. Cameron RE, Donald AM. Minimizing sample evaporation in the environmental scanning electron microscope. Journal of microscopy(Print). 1994; 173:227–237.
56. Abràmoff MD, Magalhães PJ, Ram SJ. Image processing with imageJ. Biophotonics International. 2004; 11(7):36–41.
57. Danilatos GD. Foundations of environmental scanning electron microscopy. Advances in Electronics and Electron Physics. 1988; 71:109–250.
58. Khouchaf L, Verstraete J. Electron scattering by gas in the Environmental Scanning Electron Microscope (ESEM): Effects on the image quality and on the X-ray microanalysis. J Phys IV France. 2004; 118:237–243.
59. Rose JW. Condensation heat transfer fundamentals. Chemical Engineering Research and Design. 1998; 76(2):143–152.
60. Knacke O, Stranski IN. The mechanism of evaporation. Progress in Metal Physics. 1956; 6(C)
61. Marek R, Straub J. Analysis of the evaporation coefficient and the condensation coefficient of water. International Journal of Heat and Mass Transfer. 2001; 44(1):39–53.
62. Stalder AF, Kulik G, Sage D, Barbieri L, Hoffmann P. A snake-based approach to accurate determination of both contact points and contact angles. Colloids and Surfaces A: Physicochemical and Engineering Aspects. 2006; 286(1–3):92–103.
63. Leach RN, Stevens F, Langford SC, Dickinson JT. Dropwise condensation: Experiments and simulations of nucleation and growth of water drops in a cooling system. Langmuir. 2006; 22(21): 8864–8872. [PubMed: 17014129]

Appendinx A. Nomenclature

A	Area of Liquid-Vapor Interface[m^2]
B	Area of Droplet Base[m^2]

D	Diameter of the droplet (=$2R$) [m]
D_{0i}	Diameter of the droplet in the ith frame [m]
f_s	Fraction of surface covered by adsorbed molecules
h_d	Drop-side Heat Transfer Coefficient [W/(m^{2}K)]
h_e	Interfacial Heat Transfer Coefficient [W/(m^{2}K)]
k_l	Thermal Conductivity of liquid[W/(K·m)]
$\dot{m}_l''$	Rate of Evaporative flux from the droplet [kg/(m^2·s)]
$\dot{m}_v''$	Rate of Condensation flux towards the droplet [kg/(m^2·s)]
M	Molecular Weight of the liquid [kg/mol]
$\dot{m}_0''$	Proportionality constant
p_A	Partial pressure of vapor in the gas surrounding the droplet [Pa]
P_{sat}	Saturation vapor pressure [Pa]
P_w	Modified Saturation vapor pressure[Pa]
q_d	Rate of heat transfer through droplet [W]
R	Radius of Droplet defined by Young's Laplace Equation [m]
$\bar{R}$	Universal Gas constant [J/(mol·K)]
R_0	Radius of the droplet at the initial moment of observation [m]
R^*	Critical Radius of the droplet [m]
t	Time [second]
t_{0i}	Elapsed time for the ith frame [second]
T_i	Temperature of Liquid-Vapor interface [K]
T_l	Temperature of Liquid [K]
T_s	Temperature of Sample [K]
T_v	Temperature of vapor[K]
V	Volume of Droplet [m^3]

Greek Symbols

α_c	Condensation accommodation coefficient
ρ_l	Density of Liquid [kg/m^3]
λ_s	Latent Heat of Vaporization [kJ/kg]
θ	Static Contact Angle

Appendix B. Geometrical Description of Droplet

Image analysis of droplets such as shown in Figure 6 provides measurement of the diameter in terms of its base diameter (Figure A.1).

If R_{Base} refers to the base radius of the droplet and R refers to the radius of curvature of the droplet, then a relation between these radii and their corresponding diameters can be expressed as

$$D=2R \text{ and } D_{Base}=2R_{Base} \tag{A.1}$$

As can be observed from Figure A.1, the base diameter (D_{Base}) of a droplet sitting on a substrate is related to the radius of curvature of the droplet (R). This relation can be expressed as

$$R=R_{Base}/\sin\theta \Rightarrow D=D_{Base}/\sin\theta \tag{A.2}$$

Since the analyzed images give the estimated size of base diameter, Equation A.2 was used to convert their representation in terms of base diameter to the radius of curvature. Thus the modified values of experimentally measured radii can be compared with the theoretical predictions of Equation 10, which is expressed in terms of the radius of curvature itself.

The height of the droplet sitting on a surface can be related to the radius of curvature of the droplet and the contact angle the droplet is making with the surface. This relation can be given by

$$H=R(1-\cos\theta) \tag{A.3}$$

Thus the base area of the droplet which is the substrate area covered by the droplet can be given by

$$B=\pi R_{Base}^2=\pi R^2\sin^2\theta \tag{A.4}$$

Since a droplet sitting on a surface is essentially a part of a sphere, the interfacial area and the volume of the droplet can be expressed in terms of the radius of curvature and the contact angle as

$$A=2\pi RH \Rightarrow A=2\pi R^2(1-\cos\theta) \tag{A.5}$$

and

$$V=\frac{\pi H^2(3R-H)}{3} \Rightarrow V=\frac{\pi R^3(2+\cos\theta)(1-\cos\theta)^2}{3} \tag{A.6}$$

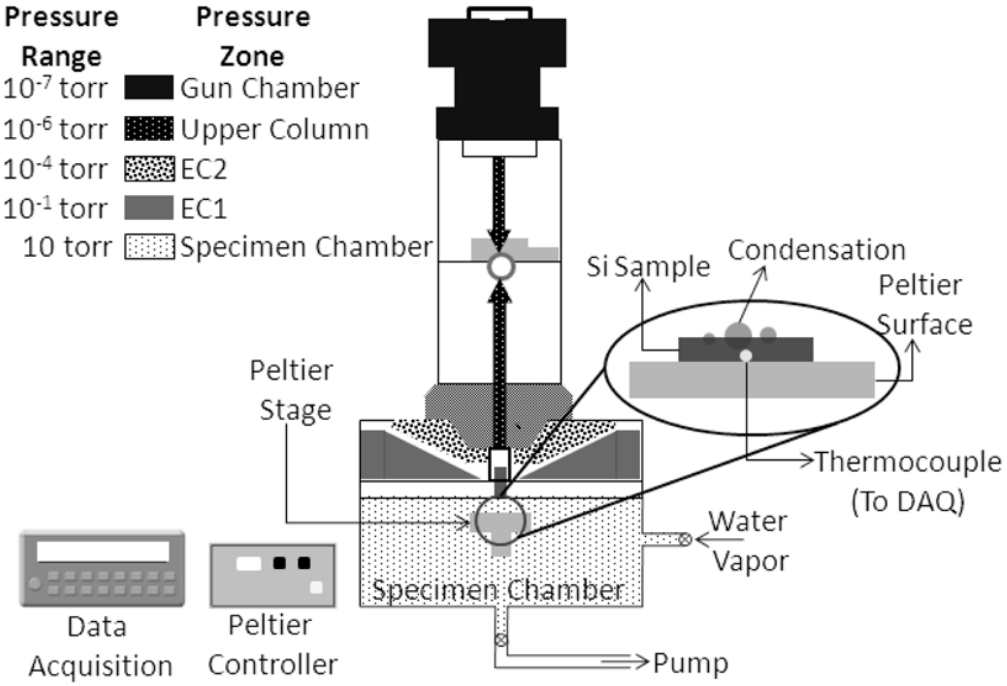

Figure 1.
Experimental Setup for Condensation Observation in ESEM

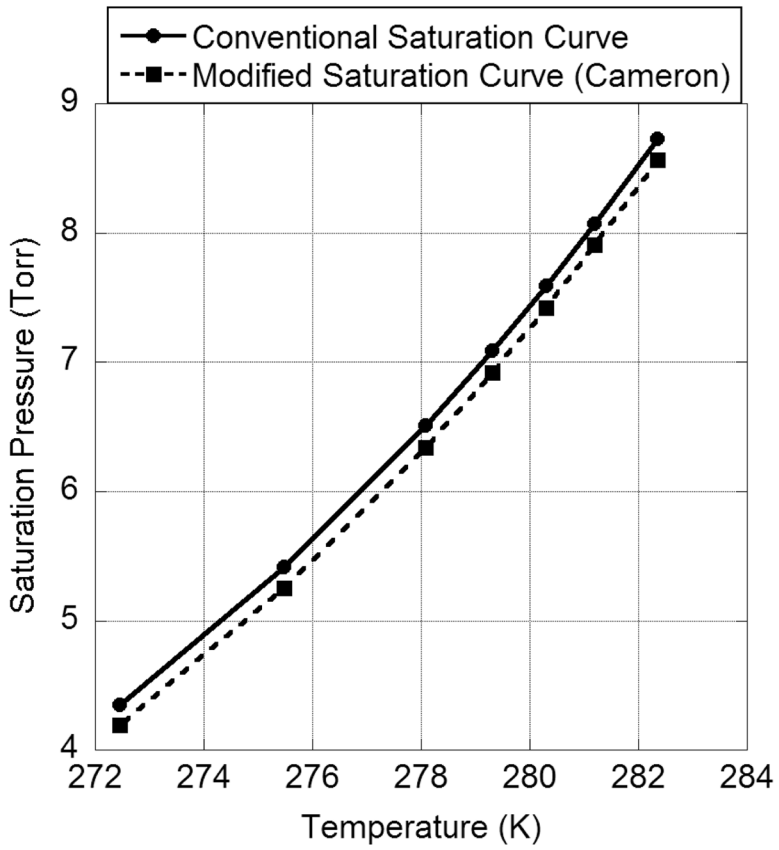

Figure 2.
Saturation Vapor Pressure – Temperature chart for ESEM

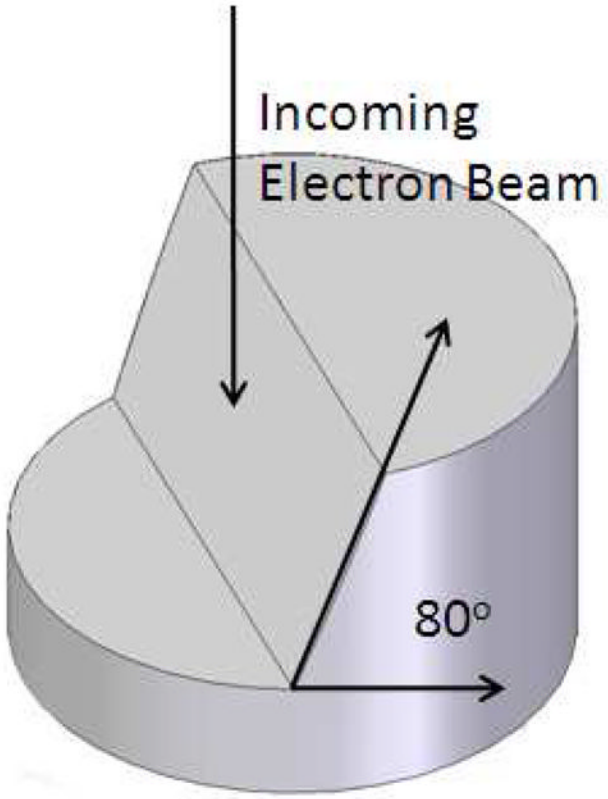

Figure 3.
Copper stage for Observing droplet condensation on an inclined surface

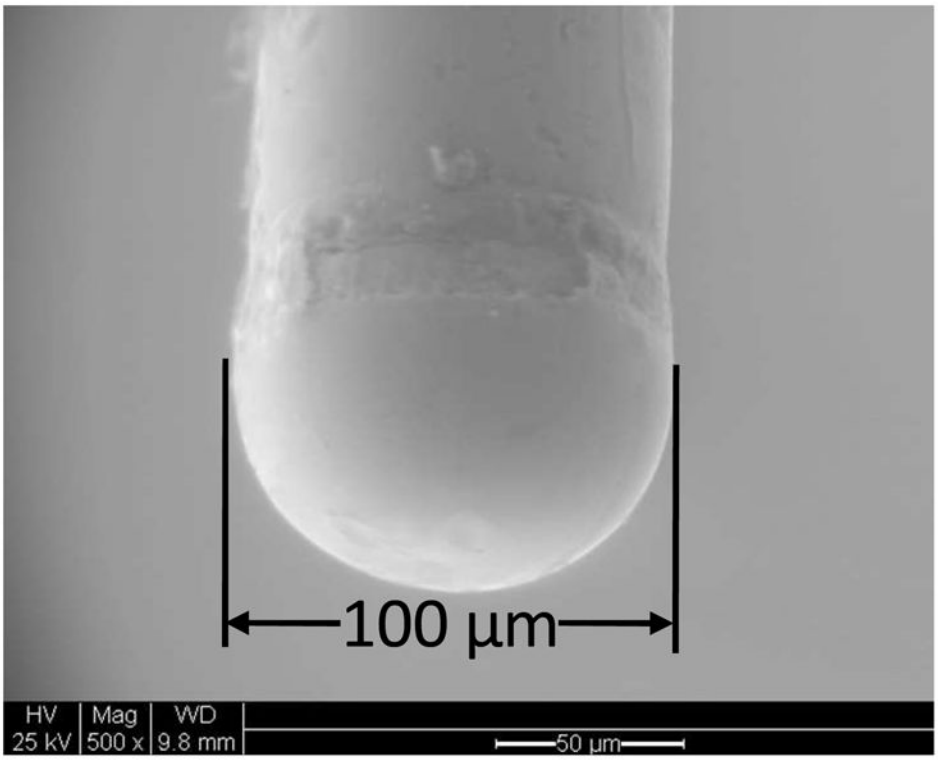

Figure 4.
Thermocouple tip

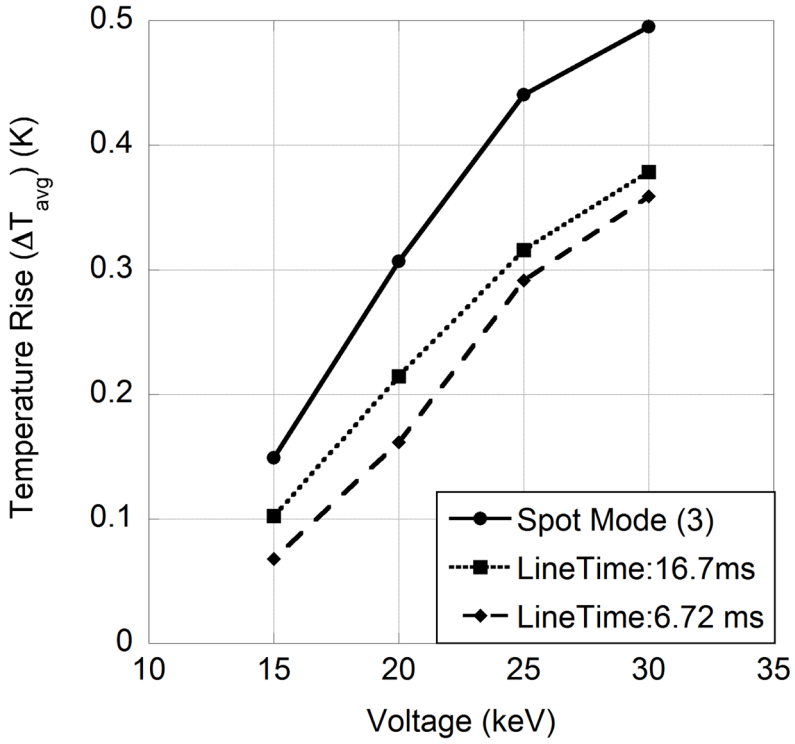

Figure 5.
Beam Heating with Beam Voltage for line mode and spot mode

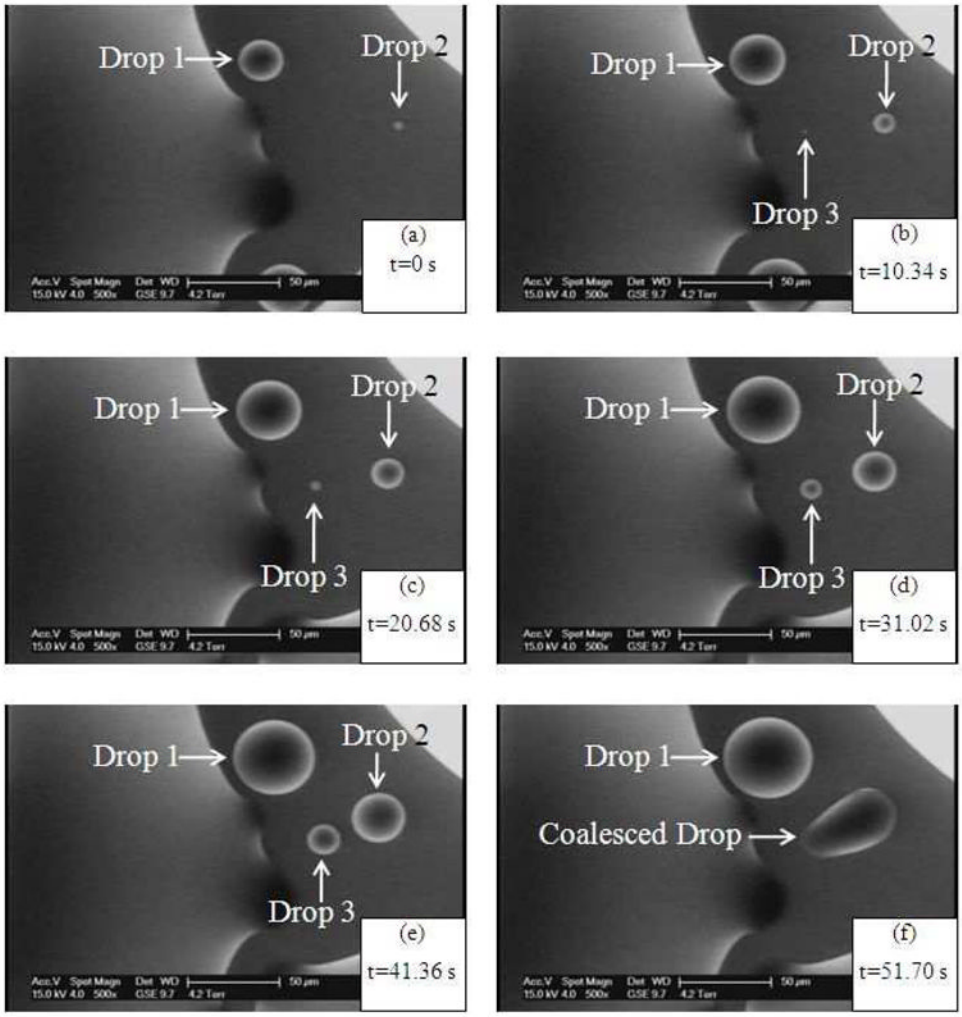

Figure 6.
Condensed droplets on Si surface (4.2 Torr) (Constant Substrate Temperature:−0.5 °C, Varying vapor pressure mode)

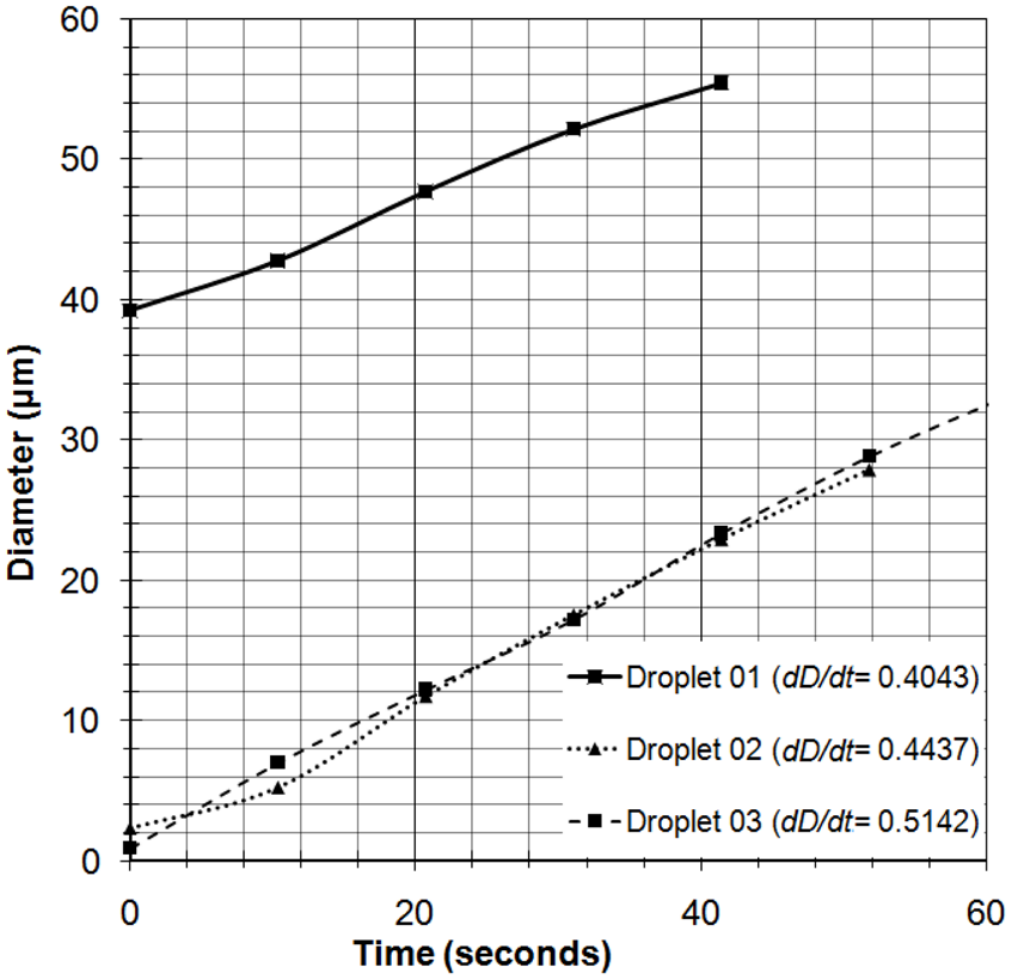

Figure 7.
Droplet diameter growth for individual droplets occurring in same frame with different initial diameters at 4.2 Torr (Constant substrate temperature, varying vapor pressure mode)

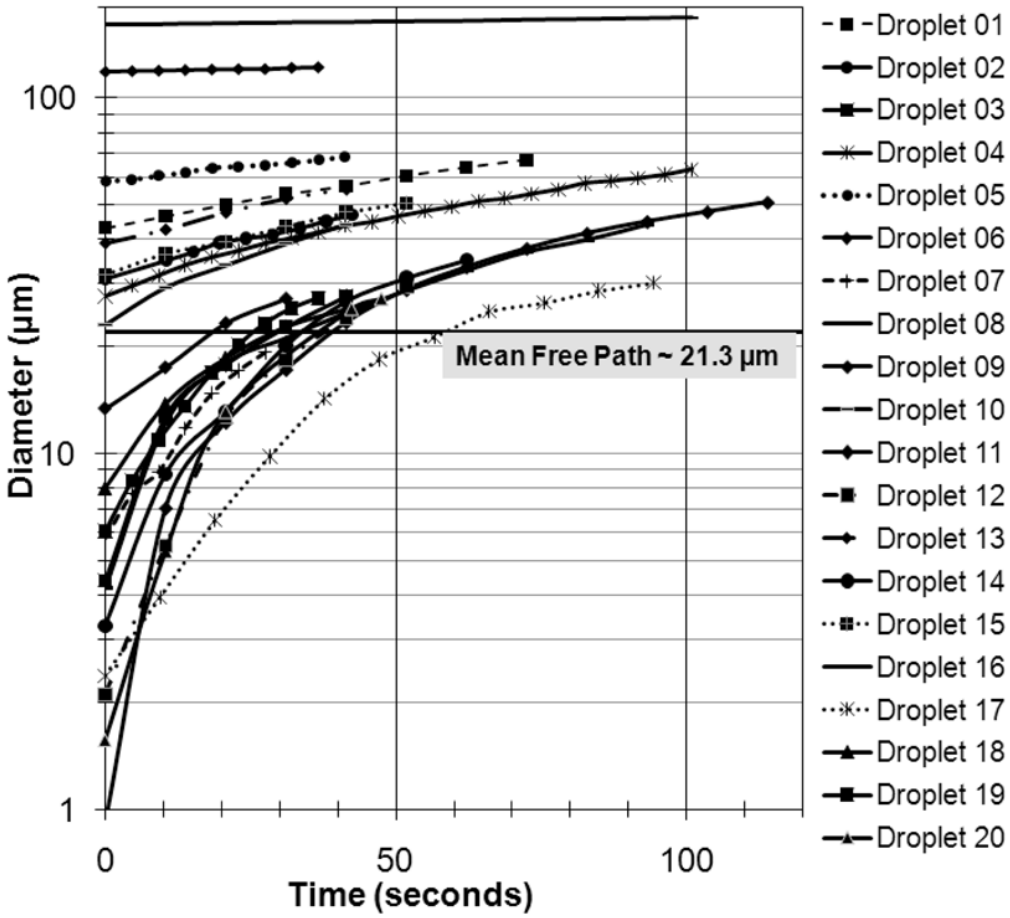

Figure 8.
Droplet growth for individual droplets

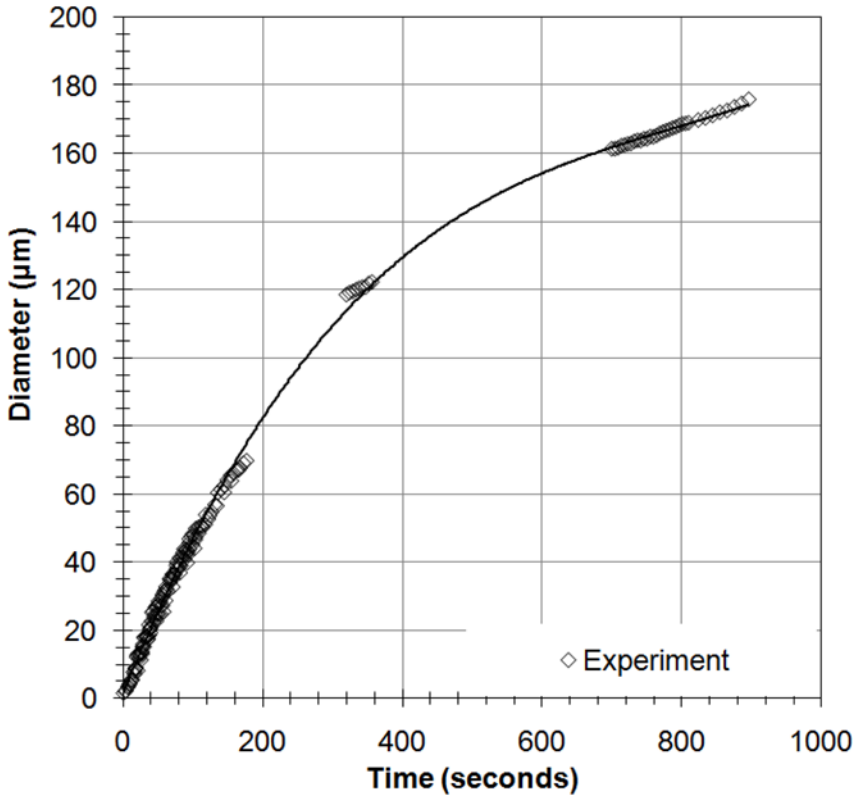

Figure 9.
Droplet growth for individual droplets evaluated for overall growth

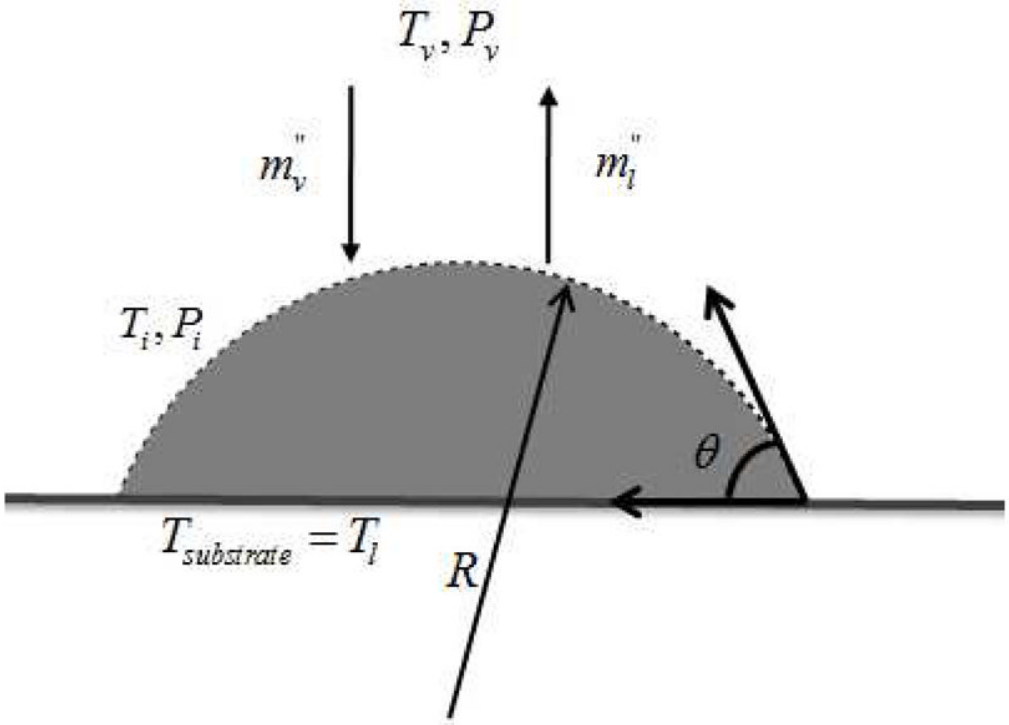

Figure 10.
Droplet on a surface

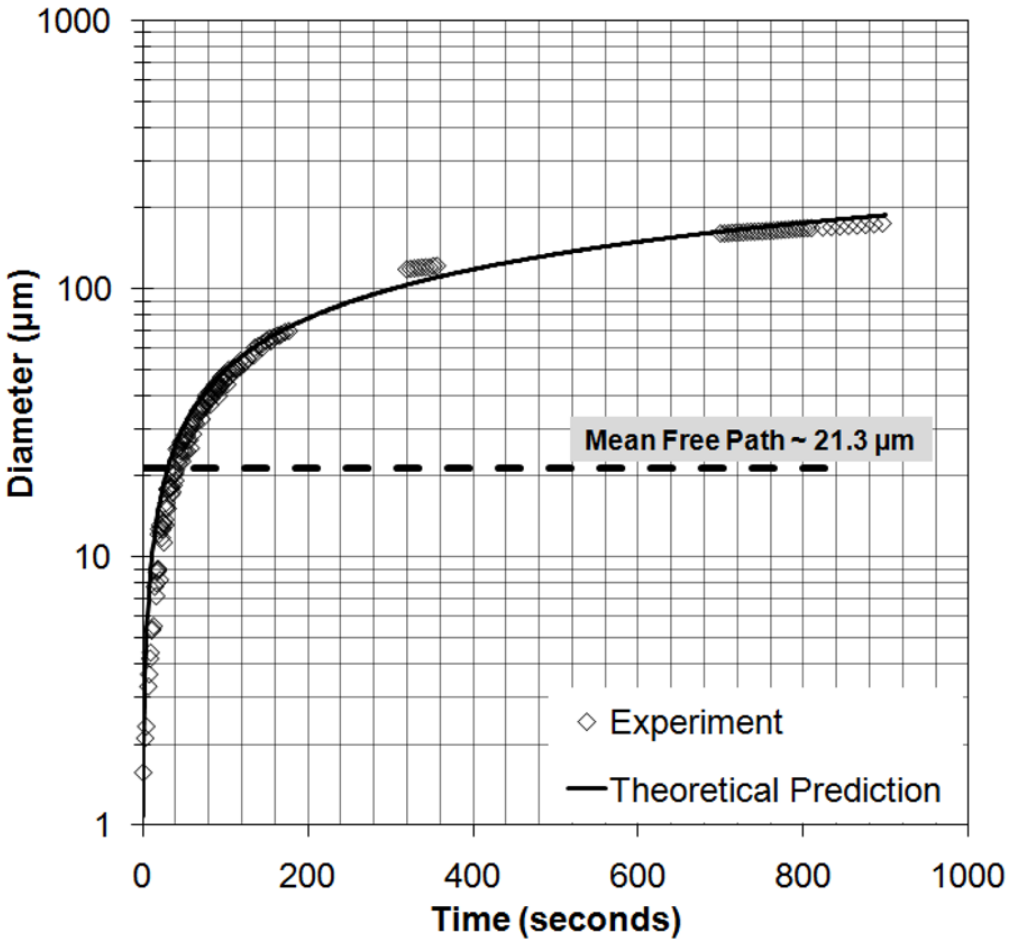

Figure 11.
Theoretical and experimental droplet growth analysis

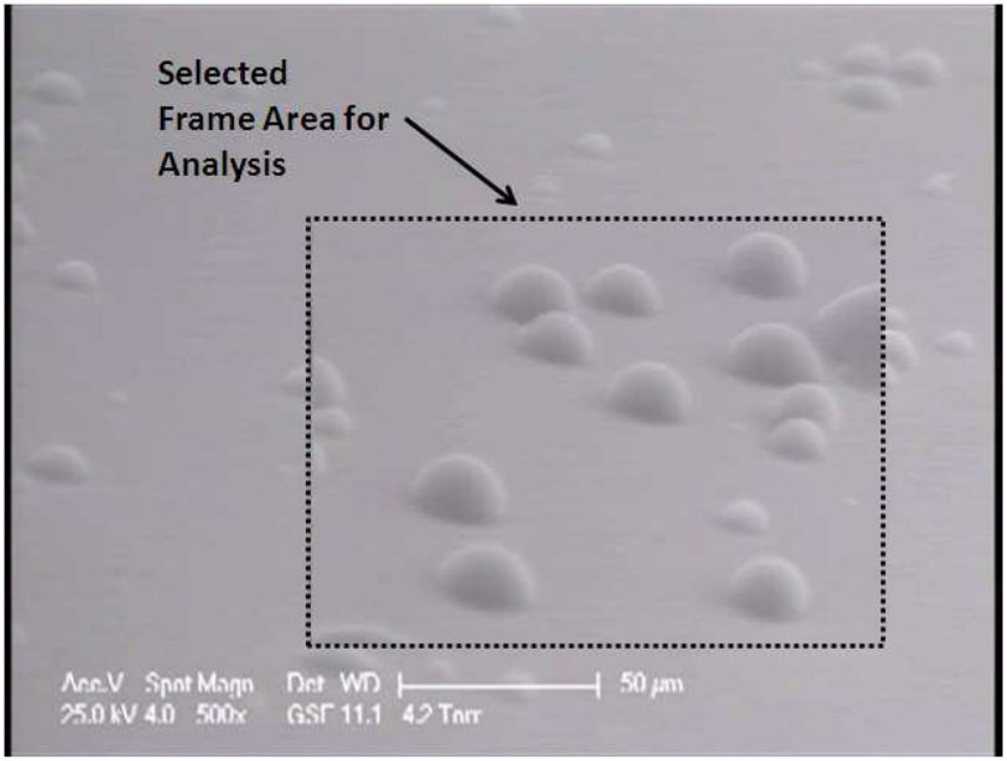

Figure 12.
Condensing droplet at 4.2 Torr visualized at 80° inclined surface (Constant substrate Temperature, Varying vapor pressure mode)

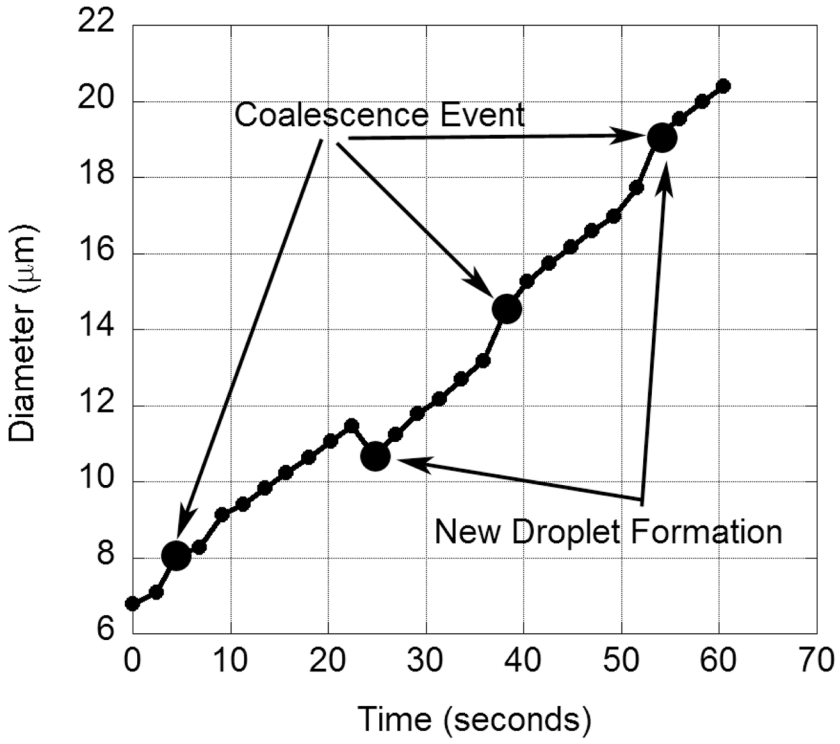

Figure 13.
Droplet Growth rate at 4.2 Torr (Constant Substrate Temperature, Varying vapor pressure mode)

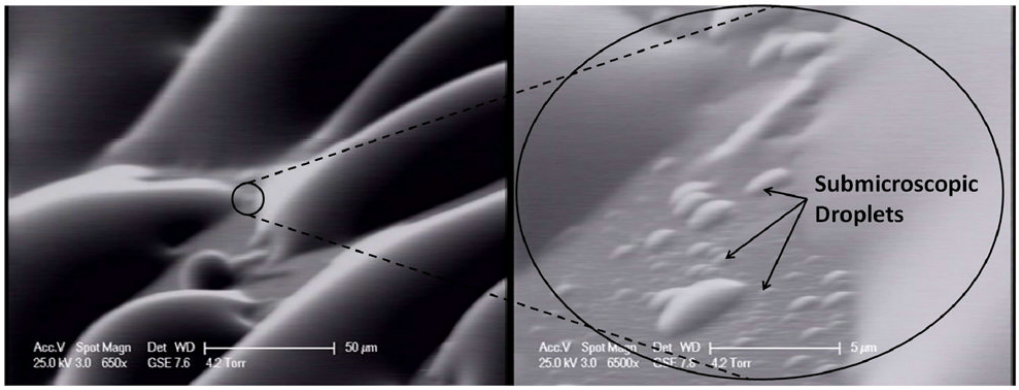

Figure 14.
Image Visualization at 6500× between visible droplets

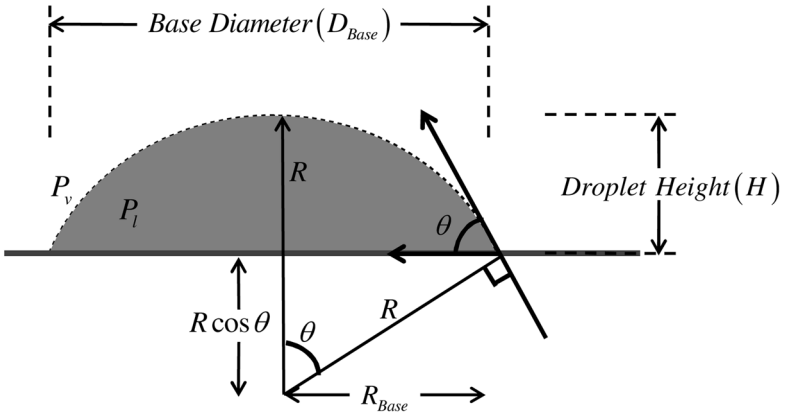

Figure A.1.
Droplet on a surface